Transport experiments on InAs self-assembled quantum dots in the microwave regime

M. S. Jun,[1,2] D. Y. Jeong,[2] S. H. Lee,[1] K. Heo,[1] J. E. Oh,[3] S. W. Hwang,[1,2,*] and D. Ahn[2]
[1]*Department of Electronics and Computer Engineering, Korea University, 5-1 Anam, Sungbuk, Seoul 136-075, Korea*
[2]*Institute of Quantum Information Processing and Systems, University of Seoul, 90 Jeonnong, Dongdaemun, Seoul 130-743, Korea*
[3]*Department of Electronic Engineering, Hanyang University, 1271 Sa-1, Sangnok, Ansan, Kyunggi-do 425-791, Korea*
(Received 12 May 2004; revised manuscript received 26 April 2005; published 4 August 2005)

We report an experimental study on microwave (MW) transport through InAs self-assembled quantum dots (SAQDs) embedded in a Au/GaAs Schottky diode. In the dc measurement, we observed isolated conductance peaks resulting from the resonant tunneling through the quantum states of the SAQDs. A single peak split into two peaks when MW signals were added. The relative strengths of these split conductance peaks changed with frequency, and it was explained by a simple convolution model including nonadiabatic electron tunneling. The inverse tunneling rate was obtained from the degree of this nonadiabacity at high frequencies.

DOI: 10.1103/PhysRevB.72.085319 PACS number(s): 73.63.Kv, 73.40.Gk

I. INTRODUCTION

A semiconductor quantum dot (QD) is an artificial atom in which the energy level can be tailored over a relatively wide range.[1] Such tailoring is achieved by nanolithographically defining planar gate patterns on high electron mobility transistor (HEMT) wafers,[2] or by etching double barrier resonant tunneling wafers into small pillars.[3] Single electron charging is a unique property of transport through QDs that facilitates probing of the energy level spectrum of QDs. Movement of the conductance peak position in the gate bias enables the detection of the energy shift due to the magnetic field (B).[4,5] This technique has also been used to identify various transitions between spin states, such as spin blockade[6] and the two-electron singlet-triplet transition in both vertical[7] and lateral[8] QDs.

Recently, the spin states in QDs have been considered an important building block for solid-state quantum computing.[9] Controlled superposition of the spin-up and spin-down states in a QD or singlet and triplet state can be a qubit. The exchange coupling between two electrons in two QDs can be adjusted to achieve SWAP gate operation.[10] The implementation and demonstration of these gate operations requires tight control of the quantum states in the time domain. The pioneering time domain experiment on a QD was the turnstile experiment by Kouwenhoven *et al.*[11] Later, measuring the dc current through a QD in the presence of a microwave (MW) signal revealed photon-assisted tunneling.[12] Microwave spectroscopy of a coupled QD molecule opens up a possibility of the charge qubit.[13] The relaxation time of a two-electron QD has been measured,[14] and recently, the operation of a charge qubit in a double QD has been demonstrated.[15]

A self-assembled QD (SAQD) is another important QD system, which is realized using one-step growth.[16] An interesting series of transport experiments examined the interplay between a layer of SAQDs and two-dimensional electron gases,[17,18] the magnetotunneling in various diodes and transistors incorporating SAQDs,[19,20] and the transport through one or a few SAQDs utilizing nanofabrication techniques.[21–23] Recently, time domain control of the quantum state evolution in SAQDs was demonstrated using optical pulses.[24] While most experimental studies have concentrated on dc and low-frequency transport, electrical transport through SAQDs in the high-frequency regime has rarely been studied.[25]

In this paper, we report an experiment that examined the transport through SAQDs embedded in a GaAs Schottky diode in a high-frequency regime. High-frequency MW signals were superimposed on the dc bias (V_{DC}) and applied to the diode. The differential conductance (dI/dV) of the diode was measured as a function of the frequency (f) and amplitude of the applied MW signals (V_{MW}). Our experiment was a two-terminal analog of the high-frequency experiment used to examine a gated QD in the classical regime.[26] The SAQD system has a random distribution of ultrasmall dots and gating is usually difficult, with very few exceptions.[27] On the other hand, the MW signal applied to the diode with a large capacitance undergoes severe attenuation. Therefore, systematic calibration of these effects is essential. In our experiment, f ranged up to 2 GHz, and the data were analyzed using nonadiabatic convolution. The tunneling rate was extracted by deriving the current in the frequency domain and by analyzing our data using the convolution theory.

II. EXPERIMENTS

Figure 1 shows a schematic of a sample and the MW measurement system. After growing a 0.6-μm-thick buffer layer with doping of 10^{18} cm^{-3} on an n+ GaAs substrate with (100) orientation, two layers of InAs SAQDs were grown inside an undoped GaAs matrix. The separation between the SAQD layers was 5 nm and the thickness of the top (bottom) undoped GaAs layers is 5 nm (6 nm). The SAQDs in the second layer are positioned automatically on top of the first-layer SAQDs because the GaAs layer covering the first layer has a greater strain right above the SAQDs.[28] All the growth occurred in a molecular beam epitaxy (MBE) chamber and the typical areal density of the SAQDs was approximately 5×10^{10} cm^{-2}. The average diameter and height of the SAQDs were 14 and 4 nm, respectively. The typical variation in the diameter is approximately 10%.[29] Additional in-

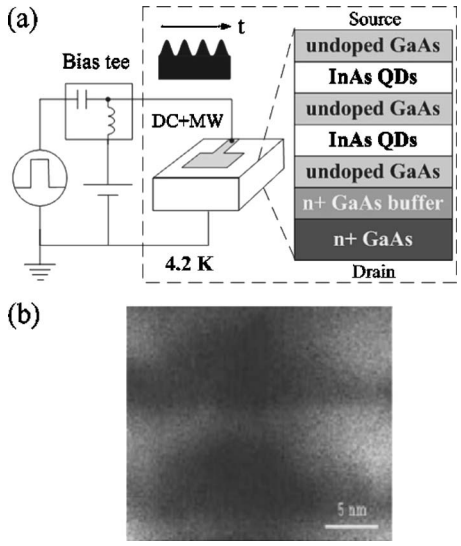

FIG. 1. Simple schematic of the measurement system and the sample structure.

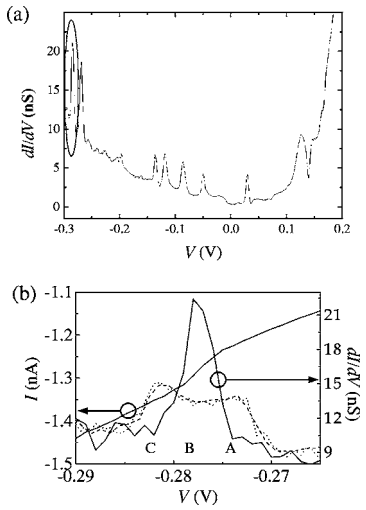

FIG. 2. (a) dc dI/dV-V characteristics. (b) Splitting of the differential conductance peak due to MW. dc I-V (solid line), dI/dV-V without MW (solid line), measured dI/dV-V with MW (dotted line, f=50 MHz), and calculated dI/dV-V with MW (dashed line).

formation on the controllability of the dot size and the uniformity has been reported elsewhere.[30]

A Ti/Au electrode was deposited on the wafer to form a Schottky contact, which can inject electrons into SAQDs when it is reverse biased.[31] The electrode was designed so that the MW signal propagates efficiently, and the area of the electrode was 1.5×10^{-3} cm^2. The backelectrode was annealed using indium for the Ohmic contact. The sample was mounted on a dip probe with superconducting coaxial cables. All the parts of the dip probe were designed so that the MW signals can propagate efficiently from the equipment at room temperature (T), to samples at low T.[32] The MW signal was transmitted to the top electrode through a superconducting coax made of Nb and polytetrafluoroethylene (PTFE),[32] and then through a microstrip transmission line designed on the TMM10i ceramic substrate[33] on which the sample was also mounted. We used a bias tee to combine V_{DC} with the MW signal. The frequency of the MW signal ranged from 40 MHz to 2 GHz. The time-averaged current (I_{TA}) was measured using a current preamplifier connected at the backcontact. We also used a low frequency lock-in to obtain dI/dV of the diode. All of the measurements were done at T=4.2 K.

Figure 2(a) shows the dc dI/dV-V characteristics of our sample measured at 4.2 K. There are several conductance peaks, and they occur when the chemical potential (μ) of the metal electrode aligns with the quantum states in the QD layers. It is difficult to exactly identify a definite quantum state corresponding to a specific resonance, since we do not know the exact value of the Schottky barrier height of our device. A strong possibility is that the peaks in the bias range $-0.2<V<0.1$ V corresponds to the low lying states such as the s and the p state, and the peaks around -0.28 V corresponds to either the d or f state. Another possibility is that only a limited number of QDs underneath the electrode are activated and each conductance peak originates from an individual QD or a small ensemble of QDs. Even in that case, our analysis discussed in the next section is still qualitatively valid.

The original motivation of having double layers was to realize a coherent oscillation between the symmetric and antisymmetric states of coupled SAQDs.[25] Our previous study of the same type of wafer, but with an n-i-n diode structure had revealed the double conductance peaks at T=20 mK, suggesting the formation of symmetric/antisymmetric states. This double conductance peak structure was compared with the calculated symmetric/antisymmetric splitting.[34] The calculated symmetric/antisymmetric splitting values ranged from 1.5 to 2.0 meV.[34] In this sample, the thermal energy ($4k_BT$) at 4.2 K (=1.2 meV) is comparable to this symmetric and antisymmetric energy level splitting. Therefore, the symmetric and antisymmetric states are overlapped and such molecular properties are not important.

We concentrated on the conductance peak at $V=-0.28$ V [circled in Fig. 2(a)], for the time-dependent measurement. Figure 2(b) shows the dc I-V (solid line), dI/dV-V without MW (solid line), measured dI/dV-V with MW (dotted line, f=50 MHz), and calculated dI/dV-V with MW (dashed line; the calculation is explained below) of the selected peak. The dc I-V and dI/dV-V without MW exhibit a single peak but dI/dV-V with MW shows split peaks. Such MW-induced peak splittings were observed in other conductance peaks but they were not clear enough to obtain a consistent set of data.

Figure 3(a) shows the amount of peak splitting as a function of V_{MW} at several different values of f in the range from 50 MHz to 2 GHz. Clearly, when f is constant, the amount of peak splitting increases linearly with V_{MW}. At the same values of V_{MW}, however, the amount of peak splitting decreases with increasing f. Figure 3(b) shows that the ratio of the peak splitting to the value of V_{MW} is inversely proportional to f. In our measurement system, there is an impedance matching condition between the superconducting coax and the waveguide on the mounting substrate. However, there is an inevitable mismatch between the characteristic impedance of the waveguide and the input impedance of the

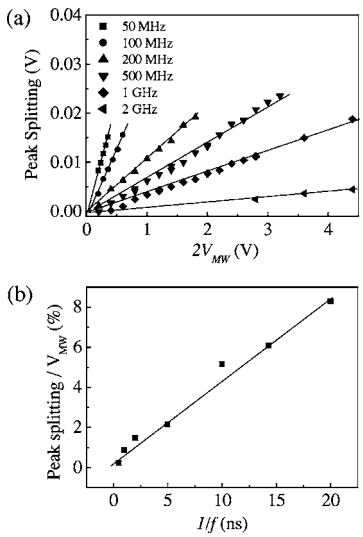

FIG. 3. (a) Peak splitting as a function of V_{MW} at various frequencies. (b) Ratio of peak splitting to V_{MW} as a function of $1/f$.

diode. The mismatch changes the input voltage of the diode with f. The impedance of the diode is a function of the external series resistance and the capacitance of the reverse-biased Schottky contact (see Appendix A). Therefore, the result in Fig. 3(b) shows a rough calibration of the effective MW amplitude (V_{eff}) from V_{MW} as a function of f. In other words, V_{eff} is the net voltage seen by the diode after losses.

Figure 4 shows the essence of our experiment. It shows the development of the split peaks as a function of f in the range from 40 MHz to 2 GHz. The applied V_{MW} values are shown together with f values in the figure. The uppermost data are the result of the dc measurement. We will compare the relative heights of the split peaks as a function of f at the same V_{eff} (the same amount of splitting). Therefore, the V_{MW} values were adjusted to maintain the same V_{eff} in all the data, using the calibration in Fig. 3(b). There was a slight drift in the V_{DC} axis from scan to scan and the data were shifted to fix the drift. Note that while the magnitude of the first peak (right peak) decreases with increasing f, the magnitude of the second peak (left peak) increases.

The appearance of the double peak structure is the result of the signal convolution.[26] Figure 5(a) schematically shows that the evenly spaced partition in the magnitude of the sinusoidal voltage gives the longest time windows at the maximum and minimum point (at $\sin \omega t = \pm 1$). Figure 5(b) shows the I-V when a MW signal is added to V_{DC}. Without MW, the current step (and the conductance peak) occurs at $V_{DC} = V_{DC}^{res}$ (The source μ is aligned with the QD energy. Note that the V_{DC} and I values are negative.). With MW, the double conductance peaks occur at particular V_{DC} values (V_{DC}^{right} and V_{DC}^{left}) where $V_{DC}^{right} - V_{eff} = V_{DC}^{res}$ ($\sin \omega t = -1$) and $V_{DC}^{left} + V_{eff} = V_{DC}^{res}$ ($\sin \omega t = 1$). At V_{DC}^{right} (V_{DC}^{left}), the resonance condition persists for the longest amount of time (near $\sin \omega t = \pm 1$). Then the time averaged current will show the steep increase at V_{DC}^{right} (V_{DC}^{left}), and we will have conductance peaks. Such scenario is valid as long as the SAQD diode can follow the time-dependent external bias adiabatically. According to this ideal model, the amount of MW-induced peak splitting is

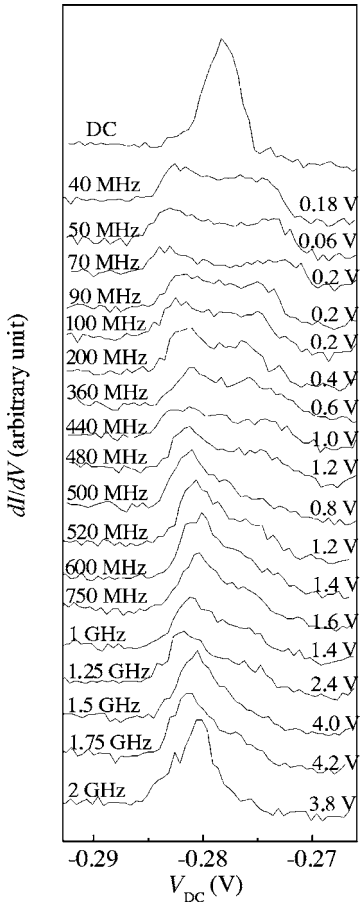

FIG. 4. Evolution of the split conductance peaks as the frequency changes from 40 MHz to 2 GHz. The listed value of V_{MW} was adjusted to maintain the same value of V_{eff} (the same amount of splitting).

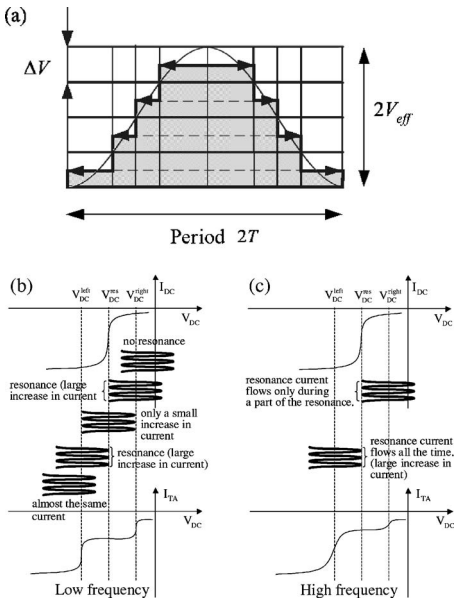

FIG. 5. (a) Segmentation of the MW signal. (b) Schematic I-V for adiabatic (left) and the nonadiabatic (right) case.

proportional to V_{MW}, as we observed in Fig. 3(a).

The change of relative heights of the split peaks at high frequency (Fig. 4) is caused by the nonadiabaticity of the tunneling electrons. At the first (right) peak, due to a finite inverse tunneling rate, the electron tunneling occurs only during a part of the time interval of the $V_{DC}^{right}-V_{eff}=V_{DC}^{res}$ condition. Therefore, the current increase becomes smaller than the lower frequency case. Such current suppression persists until $V_{DC}^{left}+V_{eff}=V_{DC}^{res}$. At this bias and above, the source μ is always higher than the quantum energy level irrespective of the sinusoidal variation. Then the diode is in the tunneling condition all the time, and the current goes back to the original dc value from the suppressed value. Therefore, a larger conductance peak occurs at this bias. In the next section, more detailed analysis is performed on this nonadiabatic tunneling, and the variation in the relative amplitudes of the split peaks as a function of f is used to obtain the characteristic time of the SAQD system.

III. ANALYSIS

A. Time-averaged current at high frequency

In this section, the MW-induced peak splitting is explained quantitatively. In an adiabatic regime, the time-averaged substrate current I_{TA} with the dc bias V_{DC}, the effective MW amplitude V_{eff}, and the frequency f ($\omega=2\pi f, 2T=1/f$) is given by

$$I_{TA}(V)=\frac{1}{2T}\int_0^{2T} I_{DC}(V_{DC}+V_{eff}\cos\omega t)dt, \tag{1}$$

$$\begin{aligned} I_{TA}(V) &\cong \frac{1}{2T}\sum_{i=-M+1}^{M} 2I_{DC}\left[V_{DC}+\left(i-\frac{1}{2}\right)\Delta V\right] \\ &\quad\times\left\{\cos^{-1}\left[(i-1)\frac{\Delta V}{V_{eff}}\right]-\cos^{-1}\left(i\frac{\Delta V}{V_{eff}}\right)\right\}\frac{2T}{2\pi} \\ &\cong \sum_{i=-M+1}^{M} I_{DC}\left[V_{DC}+\left(i-\frac{1}{2}\right)\Delta V\right]K_i, \end{aligned}$$

where $\Delta V=V_{eff}/M$, $K_i=1/\pi\{\cos^{-1}[(i-1)\Delta V/V_{eff}]-\cos^{-1}(i\Delta V/V_{eff})\}$.

As was already explained in the previous section, Fig. 5 shows the meaning of Eq. (1) schematically. Here, the amplitude V_{eff} is divided into M strips with magnitudes of ΔV. The value K_i is the normalized ith interval during which the voltage stays at the ith level. The current I_{DC} is the ideal dc tunneling current through the quantum state at a given bias level plus the background current. The calculated dI/dV-V in Fig. 2(b) is obtained from Eq. (1) and the measured I_{DC}; it reproduces the measured results qualitatively, suggesting that the simple convolution is valid in our sample.

The change in the relative peak height with f in Fig. 4 can be modeled using an equation similar to Eq. (1). The convolution in the adiabatic regime [Eq. (1)] corresponds to the case when $f\ll 1/\tau$ (I_{DC} is used). When f is larger, we define the nonadiabacity factor, δ (see Appendix B for the derivation of δ) and can modify Eq. (1) to obtain the convolution in the nonadiabatic regime

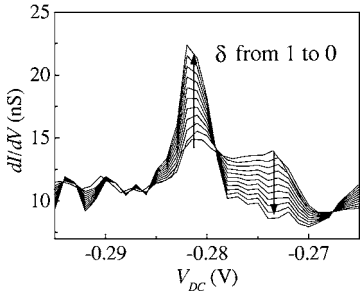

FIG. 6. Calculated dI/dV-V at several different δ values.

$$\delta=\frac{2\tau(e^{-T/\tau}-1)}{T(1+e^{-T/\tau})}+1(\textit{nonadiabacity factor}),$$
$$\frac{1}{\tau}=\frac{1}{\tau_S}+\frac{1}{\tau_D}(\textit{characteristic time}), \tag{2}$$

$$\begin{aligned} I_{TA}=&\sum_{i=-M+1}^{M-1}\delta K_i I_{DC}\left[V_{DC}+\left(i-\frac{1}{2}\right)\Delta V\right] \\ &+\left(1-\sum_{i=-M+1}^{M-1}\delta K_i\right)I_{DC}\left(V_{DC}+V_{eff}-\frac{V_{eff}}{2M}\right). \end{aligned} \tag{3}$$

Here, τ_S and τ_D are the inverse tunneling rate of the drain and the source. The effect of nonadiabacity is included by considering the fact that the electrons can tunnel from the source to the drain through the SAQD only during a decreased normalized time interval δK_i [the first term of Eq. (3)] in a period. The current stays at the minimum bias value for the rest of the time interval [the second term in Eq. (3)]. Figure 6 shows the calculated dI/dV-V using δ as a parameter. Equation (3) and the measured dc I-V data shown in Fig. 2(b) are used for the calculation. As the nonadiabacity factor changes from 1 (low frequency limit) to 0 (high frequency limit), the height of the left peak increases and the height of the right peak decreases.

B. Estimation of the tunneling rates

Measuring only I_{DC} gives the sum of the inverse tunneling rates ($\tau_S+\tau_D$). We can obtain individual values of τ_S and τ_D by obtaining δ at each frequency and by extracting the characteristic time τ.

Figure 7 shows δ as a function of $1/f$, obtained by com-

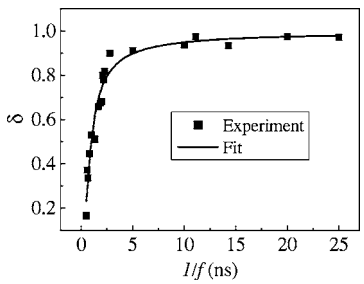

FIG. 7. Extracted δ as a function of $1/f$.

paring the relative height of the two measured conductance peaks in Fig. 4 with the calculated result in Fig. 6. The solid line is the result of fitting δ using Eq. (2). The value of τ obtained from this fitting is approximately 130 ps.

The dc current step in Fig. 2(b) is about 100 pA. The sum of τ_S and τ_D is calculated from this measured dc current step using Eq. (B10) in Appendix B and the number of SAQDs. Based on the QD density and the area of the top electrode, there are approximately 7.5×10^7 SAQDs. Therefore, considering the case when all the QDs underneath the top electrode participate in the tunneling current, the sum of τ_S and τ_D calculated from Eq. (B10) is approximately 100 ms. Using τ obtained from Fig. 7 and $\tau_S+\tau_D$, we obtain 130 ps for τ_S and 100 ms for τ_D.

The depletion region width of 51 nm can be deduced from the typical capacitance formula using the capacitance value obtained in Appendix A, the permittivity of GaAs, and the area (1.5×10^{-3} cm^2) of the material. Such a large depletion layer increases the effective barrier thickness of the backside, resulting in a large τ_D. The inverse tunneling rate of another structure with a similar barrier thickness of 45 nm was reported to be 1 ms at 4.2 K.[35]

IV. CONCLUSION

We determined the tunneling rates of electrons in and out of InAs SAQDs embedded in a metal/GaAs Schottky diode. The dc dI/dV-V characteristics showed a conductance peak that originated from the resonance of the chemical potential in the metal with the quantum energy levels of the SAQDs. On applying a sinusoidal signal in the MW range superimposed on the dc bias, the measured dI/dV showed splitting of the peaks. The amount of splitting increased linearly with V_{MW} and the relative height difference of the split conductance peaks increased with the frequency. The observed peak splitting and the change in the relative peak height are explained by nonadiabatic convolution of the I-V through the SAQDs. The extracted inverse tunneling rate was $\tau_S=130$ ps and $\tau_D=100$ ms when we assumed all the SAQDs under the top electrode were participating in the transport. The large value of τ_D is consistent with the increase in the effective barrier width originating from the depletion layer of GaAs.

ACKNOWLEDGEMENTS

This work was supported by the Korean Ministry of Science and Technology and Korea Science and Engineering Foudation through the Creative Research Initiatives Program under Contract No. M10116000008-03F0000-03610. The work at Korea University was supported by the Brain Korea 21 Project in 2004.

APPENDIX A: MEASUREMENT OF THE CAPACITANCE OF THE DIODE

The admittance of the diode was measured at a V_{DC} value of −0.3 V (near the conductance peak) in a low frequency lock-in experiment. Figure 8(a) shows an equivalent circuit

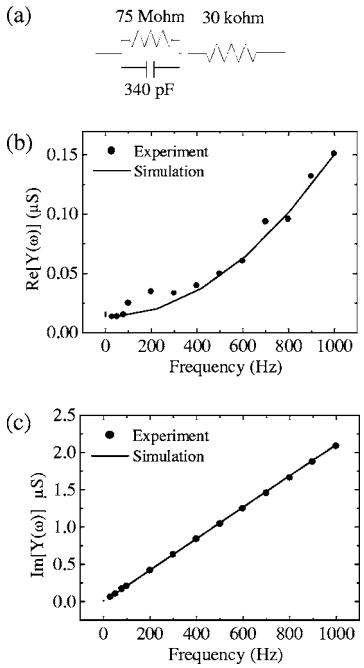

FIG. 8. (a) Equivalent circuit of our diode structure. (b) Measured and calculated real admittance of the diode. (c) Measured and calculated imaginary admittance of the diode.

model of our Schottky diode. The solid circles in Figs. 8(b) and 8(c) denote the real and imaginary part of the measured admittance, respectively. The solid lines are the fitting results using the equivalent circuit and the parameter values listed in the circuit. A large capacitance value suggests that the large attenuation at high frequency observed in Fig. 3(b) is reasonable.

APPENDIX B: DERIVATION OF δ

The added time-varying signal effectively gives the same output current whether the signal is sinusoidal or it is pulse shaped. This is because the cutoff of the current originated from the staircase structures. Figure 9 schematically shows that the output currents are the same for both a single frequency sinusoidal signal and for a pulse signal, as long as the amplitudes and frequencies are the same. Therefore, the average current due to a single frequency MW signal will be the same as that due to the pulse signal with the same frequency and the amplitude. The pulse response is much easier to solve analytically, and we derive the time-averaged current when the pulse signal is applied.

Figure 10(a) shows schematic of a two-terminal device with a QD connected between the source and the drain via tunnel barriers. Our device has a Schottky diode structure and is operated in the reverse-bias regime. The source terminal corresponds to the top metal electrode, which injects electrons at negative biases. The pulse amplitude ($2V_{eff}$) and the dc voltage are such that there is a single transition in the current during the application of the pulse. For example, we consider the case when $V_{DC}=V_{DC}^{right}(<0)$. We define $V_{low}=V_{DC}^{right}-V_{eff}$ (at resonance) and $V_{high}=V_{DC}^{right}+V_{eff}$ (off-

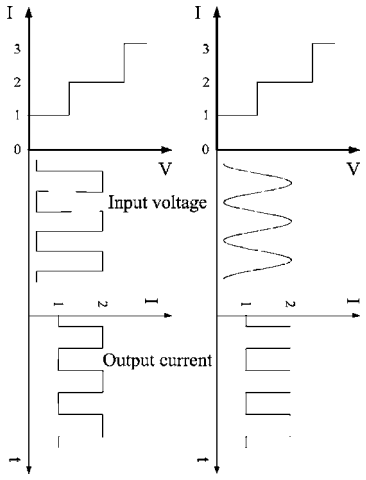

FIG. 9. Output current shape as a function of the input voltage (either sinusoidal or pulse) when the current through QD shows staircases.

resonance). Figures 10(b) and 10(c) demonstrate the pulse low and pulse high, respectively. As was already mentioned in Sec. II, the molecular properties are not important in our experiment. Either symmetric or antisymmetric level is occupied by a single electron tunneling and the two adjacent states with the nearly same tunneling rate will lead to the same result.

When P_i denotes the electron occupation probability of the ith state in the QD, the time variation of P_i is governed by the following Master equation[36,37]

$$\frac{dP_i}{dt} = \sum_{j(j\neq i)} (\Gamma_{ij}P_j - \Gamma_{ji}P_i). \tag{B1}$$

Here, Γ_{ij} is the transition rate from the jth state to the ith state. We consider only one state in the QD, and the time-dependent occupation probability of that state $P(t)$ is given by

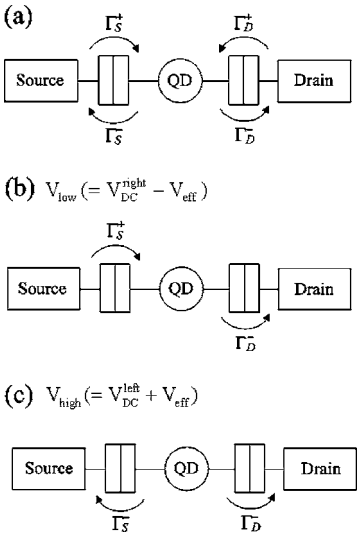

FIG. 10. Schematic of electron tunneling for the two-terminal QD system with a double barrier.

$$\frac{dP(t)}{dt} = (\Gamma_S^+ + \Gamma_D^+)(1 - P(t)) - (\Gamma_S^- + \Gamma_D^-)P(t), \tag{B2}$$

where $\Gamma_S^{\pm}$ and $\Gamma_D^{\pm}$ are the tunneling rates between the QD and the source, and between the QD and the drain, respectively. When V_{low} is applied to the source [Fig. 10(b)], $\Gamma_S^-(V_{low}) = \Gamma_D^+(V_{low}) \approx 0$ and Eq. (B2) can be rewritten as

$$\frac{dP(t)}{dt} = \frac{1-P(t)}{\tau_S} - \frac{P(t)}{\tau_D} = \frac{1}{\tau_S} - P(t)\left(\frac{1}{\tau_S} + \frac{1}{\tau_D}\right), \tag{B3}$$

where $\tau_S = 1/\Gamma_S^+(V_{low})$ and $\tau_D = 1/\Gamma_D^-(V_{low})$. Then, for the initial condition $P(t=0)=0$, the solution is given by

$$P(t) = \frac{\tau_D}{\tau_S + \tau_D}(1 - e^{-t/\tau}), \quad \left(\frac{1}{\tau} = \frac{1}{\tau_S} + \frac{1}{\tau_D}\right), \tag{B4}$$

where τ is the characteristic time of the QD system. Then, the time-dependent current $I(t)$ then is given by

$$I(t) = q\frac{P(t)}{\tau_D} = \frac{q}{\tau_S + \tau_D}(1 - e^{-t/\tau}). \tag{B5}$$

When the MW signal is switched to V_{high} at $t=T$ [Fig. 10(c)], $\Gamma_S^+(V_{high}) = \Gamma_D^+(V_{high}) \approx 0$ and Eq. (B2) now becomes

$$\frac{dP(t)}{dt} = -(\Gamma_S^- + \Gamma_D^-)P(t). \tag{B6}$$

The condition $\Gamma_S^-(V_{high}) = \Gamma_S^+(V_{low})$ is induced from Fermi's golden rule.[38,39] The tunneling (decay) time from the SAQD system to the drain is not a function of the bias, so that $\Gamma_D^-(V_{high}) = \Gamma_D^-(V_{low})$. Then, with the initial condition $[\tau_D/(\tau_S+\tau_D)](1-e^{-T/\tau})$, the solution of Eq. (B6) is $P(t) = [\tau_D/(\tau_S+\tau_D)](1-e^{-T/\tau})e^{-(t-T)/\tau}$, with the same time constant τ. When a series of these pulses are applied, the initial condition $P(t)$ at the start of the second pulse is obtained from $P(t)$ at the end of the first pulse and we can repeat similar calculations for a large number of pulses.

For a large enough n, when the start time of the nth period is $t=0$, the values of $P(t)$s for pulse low and pulse high are given by the following asymptotic forms:

$$P_{low}(t) \cong \left[\frac{\tau e^{-T/\tau}}{\tau_S(1+e^{-T/\tau})} - \frac{\tau}{\tau_S}\right]e^{-t/\tau} + \frac{\tau}{\tau_S} \tag{B7}$$

$$P_{high}(t) \cong \left[\frac{\tau e^{-T/\tau}}{\tau_S(1+e^{-T/\tau})} - \frac{\tau}{\tau_S}\right]e^{-(t-T)/\tau}. \tag{B8}$$

Here $2T$ is the period of the pulse. Then, the average current I_{avg} is given by

$$I_{ave} = \frac{I_{high}+I_{low}}{2} = \frac{q}{2T\tau_D}\left[\int_0^T P_{low}(t)dt + \int_T^{2T} P_{high}(t)dt\right]$$
$$\cong \frac{q\tau}{T\tau_D}\left[\frac{\tau e^{-T/\tau}}{\tau_S(1+e^{-T/\tau})} - \frac{\tau}{\tau_S}\right](1-e^{-T/\tau}) + \frac{q}{2(\tau_S+\tau_D)}. \tag{B9}$$

If there are N coupled QDs in the diode, the total time-average current of the diode $I_{TA} = NI_{avg}$. As this equation rep-

resents the current generated by a pulse train with the duty cycle of 50%, we expect that I_{TA} in the $T \to \infty$ limit approaches half of the dc current, I_{DC}:

$$I_{DC} = 2I_{TA}|_{T\to\infty} = \frac{qN}{\tau_S + \tau_D} = qN\frac{\Gamma_S\Gamma_D}{\Gamma_S + \Gamma_D}. \qquad \text{(B10)}$$

Therefore, the nonadiabacity factor $\delta = 2I_{TA}/I_{DC}$ can be derived as was given in Eq. (2). The derived I_{TA} here is only for the single transition to define the phenomenological δ parameter. More general form of I_{TA} was given by the convolution [Eq. (3)].

*Electronic address: swhwang@korea.ac.kr

[1] M. A. Kastner, Phys. Today **46**, 24 (1993); R. C. Ashoori, Nature (London) **379**, 413 (1996).

[2] U. Meirav, M. A. Kastner, and S. J. Wind, Phys. Rev. Lett. **65**, 771 (1990).

[3] M. A. Reed, J. N. Randall, R. J. Aggarwal, R. J. Matyi, T. M. Moore, and A. E. Wetsel, Phys. Rev. Lett. **60**, 535 (1988).

[4] P. L. McEuen, E. B. Foxman, U. Meirav, M. A. Kastner, Y. Meir, N. S. Wingreen, and S. J. Wind, Phys. Rev. Lett. **66**, 1926 (1991).

[5] O. Klein, C. de C. Chamon, D. Tang, D. M. Abusch-Magder, U. Meirav, X.-G. Wen, M. A. Kastner, and S. J. Wind, Phys. Rev. Lett. **74**, 785 (1995).

[6] P. Hawrylak, C. Gould, A. Sachrajda, Y. Feng, and Z. Wasilewski, Phys. Rev. B **59**, 2801 (1999); M. Ciorga, A. S. Sachrajda, P. Hawrylak, C. Gould, P. Zawadzki, S. Jullian, Y. Feng, and Z. Wasilewski, *ibid.* **61**, R16315 (2000).

[7] S. Tarucha, D. G. Austing, Y. Tokura, W. G. van der Wiel, and L. P. Kouwenhoven, Phys. Rev. Lett. **84**, 2485 (2000).

[8] J. Kyriakidis, M. Pioro-Ladriere, M. Ciorga, A. S. Sachrajda, and P. Hawrylak, Phys. Rev. B **66**, 035320 (2002).

[9] See, for example, a quantum information science and technology roadmap, ARDA (2002).

[10] G. Burkard, D. Loss, and D. P. DiVincenzo, Phys. Rev. B **59**, 2070 (1999).

[11] L. P. Kouwenhoven, A. T. Johnson, N. C. van der Vaart, C. J. P. M. Harmans, and C. T. Foxon, Phys. Rev. Lett. **67**, 1626 (1991).

[12] L. P. Kouwenhoven, S. Jauhar, J. Orenstein, P. L. McEuen, Y. Nagamune, J. Motohisa, and H. Sakaki, Phys. Rev. Lett. **73**, 3443 (1994).

[13] T. H. Oosterkamp, T. Fujisawa, W. G. van der Wiel, K. Ishibashi, R. V. Hijman, S. Tarucha, and L. P. Kouwenhoven, Nature (London) **395**, 873 (1998).

[14] T. Fujisawa, D. G. Austing, Y. Tokura, Y. Hirayama, and S. Tarucha, Nature (London) **419**, 278 (2002).

[15] T. Hayashi, T. Fujisawa, H. D. Cheong, Y. H. Jeong, and Y. Hirayama, Phys. Rev. Lett. **91**, 226804 (2003).

[16] D. Leonard, M. Krishnamurthy, C. M. Reaves, S. P. Denbaars, and P. M. Petroff, Appl. Phys. Lett. **63**, 3203 (1993).

[17] H. Sakaki, G. Yusa, T. Someya, Y. Ohno, T. Noda, H. Akiyama, Y. Kadoya, and H. Noge, Appl. Phys. Lett. **67**, 3444 (1995).

[18] E. Ribeiro, R. D. Jaggi, T. Heinzel, K. Ensslin, G. Medeiros-Ribeiro, and P. M. Petroff, Phys. Rev. Lett. **82**, 996 (1999).

[19] P. C. Main, A. Thornton, R. J. A. Hill, S. T. Stoddart, T. Ihn, L. Eaves, K. A. Benedict, and M. Henini, Phys. Rev. Lett. **84**, 729 (2000).

[20] E. E. Vdovin, A. Levin, A. Patane, L. Eaves, P. C. Main, Yu. N. Khanin, Yu. V. Dubrovskii, M. Henini, and G. Hill, Science **290**, 122 (2000).

[21] D. G. Austing, S. Tarucha, P. C. Main, M. Henini, S. T. Stoddart, and L. Eaves, Appl. Phys. Lett. **75**, 671 (1999).

[22] S. K. Jung, C. K. Hyon, J. H. Park, S. W. Hwang, D. Ahn, M. H. Son, B. D. Min, Y. Kim, and E. K. Kim, Appl. Phys. Lett. **75**, 1167 (1999).

[23] K. H. Schmidt, M. Versen, U. Kunze, D. Reuter, and A. D. Wieck, Phys. Rev. B **62**, 15879 (2000).

[24] N. H. Bonadeo, J. Erland, D. Gammon, D. Park, D. S. Katzer, and D. G. Steel, Science **282**, 1473 (1998).

[25] M. S. Jun, D. Y. Jeong, J. E. Oh, S. W. Hwang, and D. Ahn, Physica E (Amsterdam) **21**, 460 (2004).

[26] L. P. Kouwenhoven, N. C. van der Vaart, Yu. V. Nazarov, S. Jauhar, D. Dixon, K. McCormick, J. Orenstein, P. L. McEuen, Yu. Nagamune, J. Motohisa, and H. Sakaki, Surf. Sci. **361**, 591 (1996).

[27] A. Patanè, R. J. A. Hill, L. Eaves, P. C. Main, M. Henini, M. L. Zambrano, A. Levin, N. Mori, C. Hamaguchi, Yu. V. Dubrovskii, E. E. Vdovin, D. G. Austing, S. Tarucha, and G. Hill, Phys. Rev. B **65**, 165308 (2002).

[28] G. S. Solomon, J. A. Trezza, A. F. Marshall, and J. S. Harris, Jr., Phys. Rev. Lett. **76**, 952 (1996).

[29] S. Oh, C. Hyon, S. Sull, S. Hwang, and Y. Park, Rev. Sci. Instrum. **73**, 4687 (2003).

[30] J. W. Kim, J. E. Oh, S. C. Hong, C. H. Park, and T. K. Yoo, IEEE Electron Device Lett. **21**, 329 (2000).

[31] S. K. Jung, S. W. Hwang, B. H. Choi, S. I. Kim, J. H. Park, Y. Kim, E. K. Kim, and S. K. Min, Appl. Phys. Lett. **74**, 714 (1999).

[32] M. S. Jun, S. W. Hwang, D. Y. Jeong, and D. Ahn, Rev. Sci. Instrum. **75**, 2455 (2004).

[33] Rogers Co. Datasheet, TMM properties, http://www.rogerscorporation.com.

[34] M. H. Son, J. H. Oh, D. Y. Jeong, D. Ahn, M. S. Jun, S. W. Hwang, J. E. Oh, and L. W. Engel, Appl. Phys. Lett. **82**, 1230 (2003).

[35] G. Medeiros-Ribeiro, J. M. Garcia, and P. M. Petroff, Phys. Rev. B **56**, 3609 (1997).

[36] L. R. C. Fonceca, A. N. Korotov, K. K. Likharev, and A. A. Odintsov, J. Appl. Phys. **78**, 3238 (1995).

[37] C. F. Destefani, G. E. Marques, and C. Trallero-Giner, Phys. Rev. B **65**, 235314 (2002).

[38] C. Wasshuber, Ph.D. thesis, Technical University of Wien, Vienna, 1997.

[39] Y. Utsumi, H. Imamura, M. Hayashi, and H. Ebisawa, Phys. Rev. B **67**, 035317 (2003).